Chemical Physics 126 (1988) 191–200
North-Holland, Amsterdam

ORIENTATION OF THE CN X $^2\Sigma^+$ FRAGMENT FOLLOWING PHOTOLYSIS OF ICN BY CIRCULARLY POLARIZED LIGHT

Eckart HASSELBRINK [1], Janet R. WALDECK and Richard N. ZARE
Department of Chemistry, Stanford University, Stanford, CA 94305, USA

Received 24 May 1988

A low-pressure vapor of cyanogen iodide (ICN) is photolyzed by a beam of circularly polarized radiation at 248 nm from a KrF excimer laser. The resulting ground state CN X $^2\Sigma^+$ fragments are probed by laser-induced fluorescence (LIF) via the CN B $^2\Sigma^+$–X $^2\Sigma^+$ band system. The probe beam is directed antiparallel to the photolysis beam and is alternately left-circularly or right-circularly polarized. By analyzing the variation of the LIF signal with respect to the circular polarization of the probe light, it is deduced that the CN photofragments are oriented, that is, the CN molecules rotate in space with a preferred clockwise or counterclockwise sense. The degree of orientation varies with individual rotational levels for the CN(v=0) fragments, and the orientation even changes direction as a function of the CN rotational quantum number N. Strong evidence is presented indicating that the CN orientation direction correlates with the $^2P_{3/2}$ or $^2P_{1/2}$ fine-structure level of the iodine atom half-collision partner. The CN X $^2\Sigma^+$(v=2) fragments are formed only with ground state ($^2P_{3/2}$) iodine atoms because of energetic constraints. For these photofragments, the F_1 ($J=N-1/2$) and F_2 ($J=N+1/2$) fine-structure components appear to be nearly equally and oppositely oriented so that the net orientation vanishes unless the individual spin–rotation fine-structure components are resolved. It is proposed that spin–orbit interaction causes the photofragment orientation, in analogy to how this interaction produces spin-polarized electrons in the photoionization of atoms or molecules by circularly polarized light.

1. Introduction

Photodissociation dynamics is a subject of intense interest [1] because it concerns how bound molecules, once excited into a continuum state, evolve into separated fragments via a "half-collision" process. Whereas earlier studies often addressed the measurement of fragment scalar quantities, such as electronic state, fine-structure state, and internal state (rovibronic) population distributions, more recent work has emphasized the measurement of fragment vector quantities, such as the angular distribution of one of the fragments or the spatial distribution of the angular momentum vector of one of the fragments [2].

The production of polarized photofragments is of particular interest as a diagnostic of the half-collision dynamics [3]. Polarized angular momentum may be divided into two types: alignment and orientation. Alignment refers to even spatial moments of the fragment angular momentum vector distribution; for a diatomic fragment, alignment is equivalent to the existence of a preferred plane of rotation. Orientation refers to odd spatial moments of the fragment angular momentum vector distribution; for a diatomic fragment, orientation is equivalent to the existence of a preferred sense of rotation (either clockwise or counterclockwise).

We report here what appears to be the first observation of angular momentum orientation in a molecular photofragment. This is accomplished by photolyzing a randomly oriented sample of the linear triatomic molecule, ICN, with a beam of circularly polarized light at 248 nm. The resulting ground state CN fragment is detected by laser-induced fluorescence (LIF) with a counterpropagating beam of probe light. The degree of orientation of the CN fragment is determined by recording the intensity of the LIF signal when the probe laser beam is alternately circularly polarized with left-handed or right-handed helicity. Not only is the CN fragment found to be oriented, but the degree of orientation sensitively de-

[1] Present address: Fritz-Haber-Institut der Max-Planck-Gesellschaft, Faradayweg 4-6, 1000 Berlin 33, Germany.

pends upon the rotational state of the fragment and the direction of orientation even changes sign.

Photodissociation of ICN through its $\tilde{A}$ state continuum is of particular interest because more than one potential energy surface is involved. The photofragments are the CN radical in its ground electronic state (CN $X\,^2\Sigma^+$) and the iodine atom in its upper $I(^2P_{1/2})$ and lower $I(^2P_{3/2})$ fine-structure levels. Although molecular photofragment orientation appears to be unprecedented, it is well known that a circularly polarized beam of light can produce oriented (spin-polarized) photoelectrons in the photoionization of unpolarized samples of isolated atoms and molecules [4–6]. Probably less well known is the study by Vasyutinskii [7] on the photolysis of CsI vapor by a beam of circularly polarized light in which the ground state $Cs(6s\,^2S)$ atom was observed to show a small degree of orientation (less than a few percent). Thus, it would appear that photofragment orientation is a general phenomenon in which the helicity of the photolysis photon is transferred to the fragment angular momentum. It is the purpose of the present paper to examine the degree of orientation of the CN fragment following the photolysis of ICN by circularly polarized light and to demonstrate the power of this technique in probing photodissociation dynamics.

2. Experimental

Fig. 1 shows a schematic diagram of the experimental configuration. The ICN sample (Eastman Kodak), purified by resublimation, flows slowly through a vacuum chamber at pressures between 5–10 mTorr. The ICN molecules are photodissociated by UV light pulses form a KrF excimer laser at 248 nm and the CN $X\,^2\Sigma^+$ fragment is then probed by LIF using a tunable dye laser. The two laser beams enter the chamber collinearly but oppositely directed. Both lasers are circularly polarized and the handedness of the probe laser is reversed on alternate pulses. The fluorescence signal is collected normal to the propagation direction of the laser beams by a photomultiplier tube (RCA 7326) without any further polarization analysis. An interference filter, centered on the CN $B\,^2\Sigma^+$–$X\,^2\Sigma^+ \Delta v = 0$ sequence, serves to suppress scattered laser light.

A KrF excimer laser (Lambda Physik EMG 200) provides the photolysis light and pumps a tunable dye laser (Lambda Physik FL2002E). Prior to the excimer laser beam traversing the vacuum chamber, the excimer laser beam is recollimated by a 60 cm quartz lens and reduced in beam size by an aperture. The energy of this portion of the excimer beam is about 5 mJ/pulse. In order to obtain circular polarization, the light beam is first linearly polarized by an MgF_2 Rochon prism and then converted to circular polarization by a single Fresnel rhomb (Karl Lambrecht FR-2-272-UN)

The dye laser is tuned through the CN $B\,^2\Sigma^+$–$X\,^2\Sigma^+(1, 0)$ (358 nm) and (0, 2) (460 nm) bands utilizing PBD and coumarin 450, respectively, as laser dyes. In order to avoid saturation effects [8], the dye laser is operated at low output power, i.e. without the amplifier stage, and further attenuated by two nearly crossed Glan–Taylor prisms so that the final power is less than 1 μJ/pulse. A delay of 10 ns between photolysis and dye laser pulses is sufficient to probe nascent photofragment distributions.

A photoelastic modulator (PEM, Hinds CF4) is used to circularly polarize the dye laser light. The direction of the stress exerted on the PEM quartz crystal is set at 45° relative to the linear polarization of the dye laser beam. The amplitude of compression is regulated so that the crystal oscillates between $+\lambda/4$ and $-\lambda/4$ retardations. A trigger circuit synchronizes the excimer laser firing with this sinusoidal compression so that dye laser pulses arriving at the PEM correlate alternatively with maximum compression and decompression. This results in alternating left- and right-circularly polarized light pulses. The photomultiplier signal is processed by a gated integrator (SRS 250), and the unaveraged output of this is fed to an A/D converter and sorted by a microcomputer into two channels so that one channel accumulates the signal corresponding to one handedness of the probe light and the other accumulates the corresponding opposite handedness.

We use the same setup to determine the relative helicities of the excimer and the dye laser beams. The dye laser light passes through the polarizer which establishes the linear polarization of the dye laser output, the PEM, the Fresnel rhomb, whose original purpose was to circularly polarize the excimer laser light, and the linear polarizer for the excimer. In this

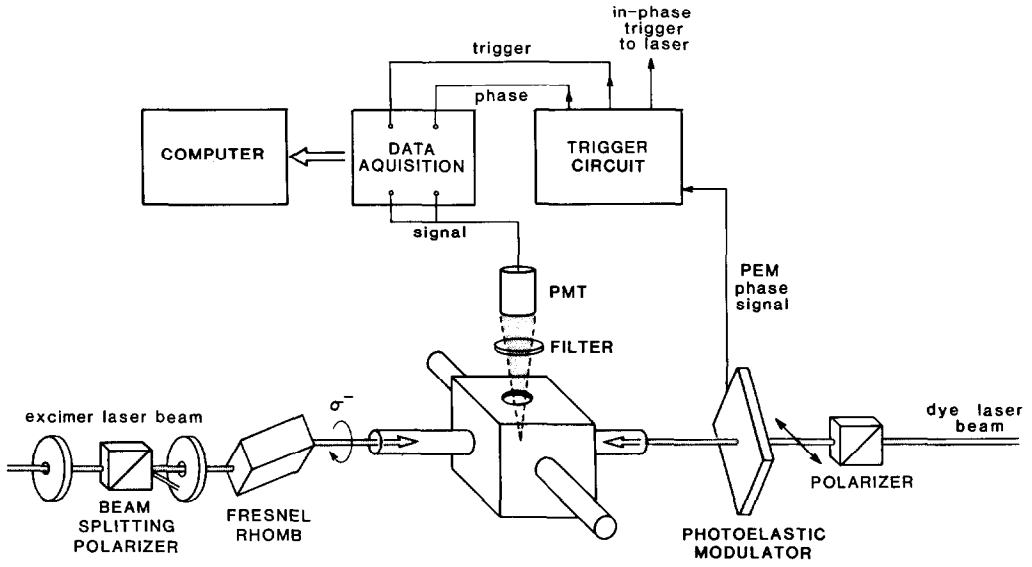

Fig. 1. Schematic diagram of the apparatus used in this study.

way the dye laser beam becomes circularly polarized by the PEM and converted to linear polarization by the Fresnel rhomb. A test for the handedness of the probe laser relative to the excimer laser is to determine whether the resulting linear polarization of the probe laser beam will be transmitted by the excimer laser's linear polarization analyzer (Rochon prism). The situation in which the final polarizer is crossed against the polarization of the light pulses is analogous to a Faraday isolator and indicates that the laser light from the (excimer) pump and (dye) probe lasers have opposite helicities. Because the laser beams travel in antiparallel directions, the photon angular momenta point for that situation in the same direction, i.e. the electric field vectors rotate in synchrony. We will label signals obtained in this case by $I_{\uparrow\uparrow}$, otherwise by $I_{\uparrow\downarrow}$.

The bandwidth of the dye laser is $\approx 0.2\ \mathrm{cm}^{-1}$ and can be narrowed to $\approx 0.07\ \mathrm{cm}^{-1}$ with an intracavity etalon. The data have been obtained by slowly scanning the broadband dye laser over the Doppler-broadened line profiles. The polarization dependence has been determined by summing the signal over the whole width of the line. This procedure excludes any unwanted effects arising from partially resolved Doppler profiles [9,10] or fine-structure splittings [11,12].

3. Results

We observe a strong orientation of the CN fragment rotation and a marked variation with the rotational state N. Figs. 2 and 3 show the signal obtained at the band origin and the (1, 0) bandhead of the CN B–X spectrum. The continuous and dashed lines indicate the signals recorded for $I_{\uparrow\uparrow}$ and $I_{\uparrow\downarrow}$, respec-

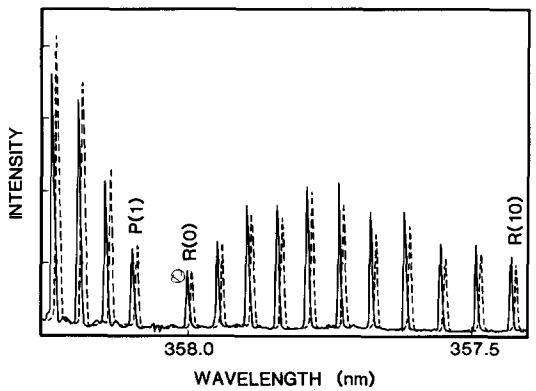

Fig. 2. Laser-induced fluorescence signals around the origin of the CN $B\,^2\Sigma^+$–$X\,^2\Sigma^+$ (1, 0) band. The solid line corresponds to the case when dissociating and probing photons have the same helicity; the dashed line corresponds to the case of opposite helicity. The two curves have been shifted against each other for clarity.

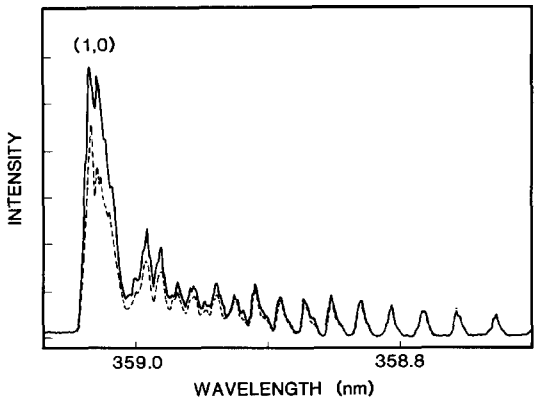

Fig. 3. Laser-induced fluorescence signal at the (1, 0) bandhead of the CN $B\,^2\Sigma^+$–$X\,^2\Sigma^+$ transition. The labeling is the same as in fig. 2.

tively. The bandhead occurs within the P branch at $N=40$. Better quantitative data can be obtained by probing the R-branch lines because in this case no lines are blended. We have taken data up to $N=55$, which is close to the limit of states populated by the photodissociaton process.

Changing the probe laser beam from left-circular to right-circular polarization yields a pair of signals whose difference is proportional to the orientation of the rotational angular momentum of the CN fragment. Phenomenologically we define the degree of circular polarization [13], $C(N)$, as

$$C(N)=\frac{I_{\uparrow\uparrow}(N)-I_{\uparrow\downarrow}(N)}{I_{\uparrow\uparrow}(N)+I_{\uparrow\downarrow}(N)}. \qquad (1)$$

We also refer to $C(N)$ as the degree of orientation. Our data show that high rotational states are oriented oppositely to low rotational states, with the observed difference in intensity reaching as much as 30% (see fig. 4). An experimental result with positive sign for an R line indicates that the CN molecular photofragment rotates in the same sense that the electric vector of the photolysis beam rotates [14,15]. In this manner, we find for low rotational quantum numbers a favored orientation of the rotational angular momentum which is antiparallel to the angular momentum of the dissociating photon, whereas for high rotational states, the parallel case is preferred. Around $N=22$ occurs a transitional region where $C(N)$ passes through zero and changes sign.

We have performed several tests to check for artifacts in our results. Comparison of R-branch lines versus P-branch lines show opposite effects because the transition moments of these lines have an opposite dependence on M_N – the projection quantum number of N. We have used this to confirm our results for low rotational quantum numbers up to $N=22$ where the P-branch lines are not blended. Within our experimental uncertainty of about ± 0.025 for $C(N)$, we find opposite results. Changing the helicity of the photolysis laser should reverse all signs of the primarily observed results. We also find that this check is fulfilled. In addition, tests have been made to ensure that the observed degree of orientation, $C(N)$, is independent of the intensity of the probe laser as well as the photolysis laser beams over the intensity range in which data were recorded.

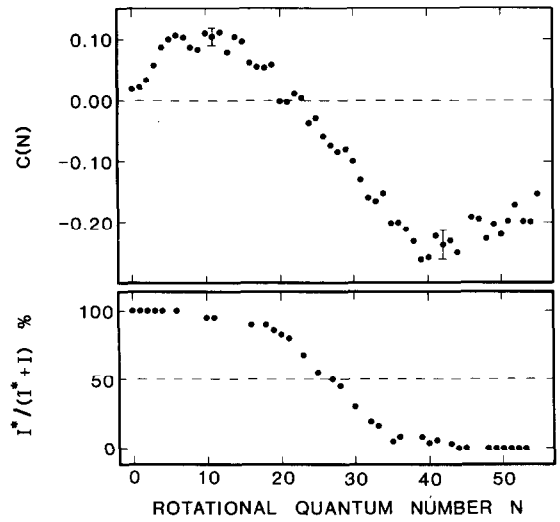

Fig. 4. Observed degree of orientation $C(N)$ versus final rotational state N of the CN($v=0$) fragment (upper panel). The lower panel shows the branching into $I(^2P_{3/2})$ and $I(^2P_{1/2})$, as obtained by Nadler et al. [11] for photodissociation at 266 nm. The curve ranges from almost exclusive population of $I(^2P_{1/2})$ for low N to almost exclusive population of $I(^2P_{3/2})$ at high N.

Under our experimental conditions in which the CN fragment is detected independent of the internal state and velocity of the I fragment, no orientation should be observed when linearly polarized light is used for photodissociation owing to reflection symmetry in the system. When the output of the photolysis is linearly polarized, we measure consistently no significant difference when probing with left-circularly or right-circularly polarized light. We therefore

conclude that the observed signal differences are caused by the orientation of the CN fragment produced in the photolysis of ICN with a beam of circularly polarized light.

Nadler et al. [11] have used CN photofragment Doppler profiles to determine the relative population of ground state and excited state iodine associated with each individual CN rotational state. Their results obtained for photodissociation at 266 nm establish that low rotational states correlate with the formation of excited iodine, whereas higher rotational states correlate with ground state iodine. Their findings are shown in the lower panel of fig. 4. Obviously the branching into $I(^2P_{3/2})$ and $I(^2P_{1/2})$ tracks the degree of orientation of the CN fragment we observe. The slight shift between both curves might well be caused by the different photolysis wavelengths used in these two experiments.

This result raises the question whether the intermediate rotational states, for which we observe small or no orientations, are themselves without orientation or are a superposition of two cancelling opposite orientations. The latter might come about from two ensembles – one connected with $I(^2P_{1/2})$ and the other with $I(^2P_{3/2})$ – each being oriented but in opposite directions and therefore resulting in a net zero effect. We therefore performed an additional experiment, namely, we examined the R(22) line with sub-Doppler resolution. For this particular state the unresolved line shows no orientation, and we expect equal populations in the $I(^2P_{3/2})$ and $I(^2P_{1/2})$ channels.

CN fragments formed with $I(^2P_{3/2})$ have 6310 cm^{-1} more excess energy than those formed with $I(^2P_{1/2})$. This excess energy shows up as a higher translational velocity of the recoiling fragments [11]. By scanning over the Doppler profile it is possible to separate, in part, the contributions from the different iodine atom spin–orbit channels, although this analysis is complicated by possible velocity angular momentum correlations [9,10]. For a parallel transition, the collinear geometry provides less resolution of the two iodine atom fine-structure levels than the crossed geometry. Nevertheless, we must use the collinear geometry to be able to study orientation.

For the wings of the line we have only a contribution from CN formed with ground state iodine, whereas in the center of the line we test a mixture with a larger contribution from CN formed with excited iodine. If the assumption holds that the orientation depends strictly on the state of the iodine atom formed during the photodissociation process, we expect the degree of orientation to be negative in the wings of the line (where $I(^2P_{1/2})$ does not contribute) and to show a small positive value in the center of the line. This is exactly what we observe experimentally (see fig. 5).

The solid line in fig. 5 is the result of a simulation in which it is assumed that the two contributions have equal but opposite degrees of orientation with the magnitude $|C(N)| = 0.15$. We have calculated the individual Doppler profiles and summed the contributions from the two iodine atom spin–orbit channels and the two CN radical spin–rotation states. Finally, we have carried out a convolution over our estimated experimental resolution (0.07 cm^{-1}). We take this experiment as strong evidence that the CN($v=0$) orientation is indeed a strict reflection of the state of the iodine atom half-collision partner in the photolysis of ICN.

So far we have exclusively reported data obtained for the $v=0$ state of CN. We have also looked at the CN($v=2$) state for which only $I(^2P_{3/2})$ atoms are observed. Here we are not able to detect orientation for unresolved lineshapes. However, for higher rotational quantum numbers ($N>40$), we are able to resolve the spin–rotation splitting because the amount of available translational energy decreases and this

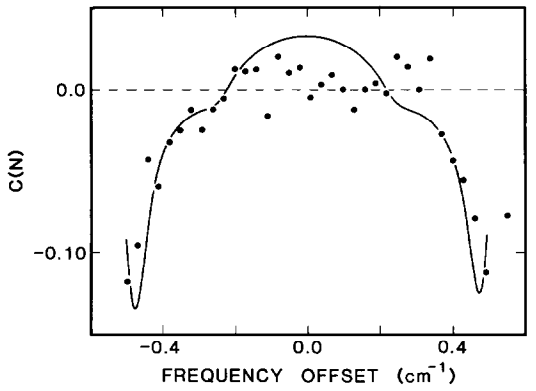

Fig. 5. Observed degree of orientation $C(N)$ versus frequency offset within the Doppler profile of the R(22) line of the CN B–X(1, 0) band. The solid curve is the result of a simulation assuming opposite orientations for the contributions from the two iodine fine-structure levels.

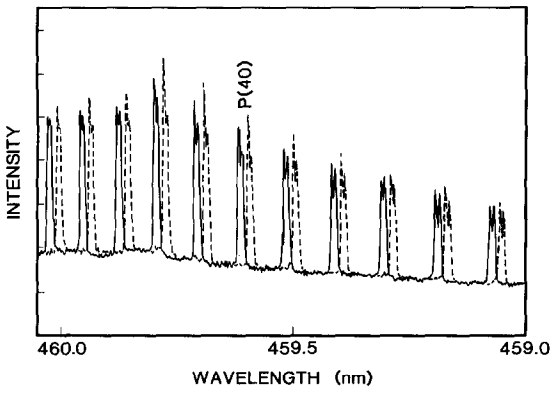

Fig. 6. Laser-induced fluorescence signal for CN(v=2). Shown are the lines P(35) to P(45). Note the different orientation of the spin–rotation components. The solid line corresponds to the case when dissociating and probing photons have the same helicity; the dashed line corresponds to the case of opposite helicity. The two curves have been shifted against each other for clarity.

fine-structure splitting increases with N. We find opposite orientations of the F_1 ($J=N-1/2$) and F_2 ($J=N+1/2$) fine-structure components (see fig. 6). No detailed quantitative analysis of the data was attempted.

4. Determination of the orientation moment $A_{0+}^{\{1\}}(N)$

One wishes to characterize the spatial angular momentum distribution of a photofragment under study as completely as possible [3]. Ideally, this would involve specifying the population of each magnetic sublevel. However, in general the use of resonance fluoresence measurements does not permit this. This topic has been considered in detail by several authors [15–17]. We follow here the treatment of Kummel, Sitz and Zare [15] (hereafter denoted by KSZ LIF) who developed formulas for the most general case of the LIF signal for a $J_i \rightarrow J_e$ probe transition followed by the unresolved detection of all possible $J_e \rightarrow J_f$ fluorescent transitions using a fixed excitation–detection geometry with no polarization analysis.

This approach makes use of the expansion of the density matrix into state multipole moments $A_{q\pm}^{\{k\}}$, which are most suitable for describing the information obtained by optical polarization analysis. Here the brackets { } around the rank k indicate that we are using the Hertel–Stoll normalization [18] in which the $A_{q\pm}^{\{k\}}$ are real and transform as the "real" spherical harmonics in the limit of large N.

Fortunately, single-photon photodissociation cannot introduce into the photofragment angular momentum distribution any moments greater than $k=1$ for orientation and $k=2$ for alignment (provided our detection system is not sensitive to angular momentum/velocity correlation of the photofragments [3]). Furthermore, the cylindrical symmetry in our experimental arrangement excludes all moments with q not equal to 0. Therefore, in our case the angular momentum distribution is completely characterized by three moments – specifically, $A_{0+}^{\{0\}}$, $A_{0+}^{\{1\}}$ and $A_{0+}^{\{2\}}$. This high degree of symmetry greatly simplifies the analysis compared to the general case where a large number of moments must be considered.

In the present experiment the probe light propagates along the $-z$ axis and the detector is situated along the y axis, where the z axis is the natural quantization axis for describing the spatial distribution of the rotational angular momentum N of the CN $X\,^2\Sigma^+$ fragment. This is called the case I geometry in KSZ LIF. For this excitation–detection geometry, a measurement of the degree of circular polarization, $C(N)$, may be related to the moments of the photofragment angular momentum distribution by

$$\frac{A_{0+}^{\{1\}}(N;\,\text{apparent})}{A_{0+}^{\{0\}}(N;\,\text{apparent})} = \frac{C(N)\,P_{0+}^{\{0\}}(N)}{P_{0+}^{\{1\}}(N)}\,, \tag{2}$$

where the $P_{0+}^{\{0\}}(N)$ and $P_{0+}^{\{1\}}(N)$ are line strength moments which are readily evaluated [#1]. (Note that the $P_{q\pm}^{\{k\}}(N)$ are not only dependent on N but also on the branch (P or R) chosen for the detection scheme.) As shown in KSZ LIF,

$$A_{0+}^{\{1\}}(\text{apparent}) = A_{0+}^{\{1\}} = \langle N|N_z/N|N\rangle \tag{3}$$

and

$$A_{0+}^{\{0\}}(\text{apparent}) = A_{0+}^{\{0\}} + a(N)A_{0+}^{\{2\}}$$

$$= 1 + a(N)\langle \mathrm{N}|\,(3N_z^2/N^2-1)\,|N\rangle\,. \tag{4}$$

Thus we can readily convert the degree of circular po-

[#1] The actual calculation of the line strength factors takes into account the effects of fine-structure and hyperfine-structure depolarization.

larization, $C(N)$, to the dipole orientation moment, $A_{0+}^{\{1\}}(N)$, with a knowledge of the line strength moments, $P_{0+}^{\{1\}}(N)$ and $P_{0+}^{\{0\}}(N)$, if it were not for the fact that the apparent population moment, $A_{0+}^{\{0\}}(N;\text{apparent})$, contains a contribution from the quadrupole alignment moment, $A_{0+}^{\{2\}}(N)$. However, as will be shown in what follows, this extra term is rather small.

From table 4 of KSZ LIF, it is seen for case I geometry that $a(N)=P_{0+}^{\{2\}}(N)/P_{0+}^{\{0\}}(N)$ has the value 0.117 for the $N=20$ R-branch member. Moreover, we have data which show that $A_{0+}^{\{2\}}$ is about 0.15. We determined in a separate experiment the alignment $A_{0+}^{\{2\}}(N)$ of the CN fragment's rotational angular momentum distribution over the range of N of interest, taking care to maintain the definition of the z axis to be along the propagation direction of the photolysis laser beam. This experiment used a crossed laser beam geometry. The photolysis laser was circularly polarized and the probe laser linearly polarized. The direction of the electric field vector of the latter was alternated between being parallel to and perpendicular to the propagation direction of the photolysis laser.

The data obtained in this way agree well with the alignment data obtained in an earlier experiment [19]. We measure consistently $A_{0+}^{\{2\}}(N)$ to have the value of 0.15 without much variation with N. Hence, the contribution of the quadrupole alignment moment to the apparent population moment introduces a correction in the dipole orientation moment of less than 3%.

Fig. 7 shows the values of $A_{0+}^{\{1\}}(N)$ which were obtained on the basis of our data. The curve follows basically the form of the degree of circular polarization found previously.

With a knowledge of all three moments, we have achieved the ideal situation of having a complete description of the angular momentum distribution. We use the well-known inverse expansion of the density matrix in state multipole moments $A_q^{(k)}(N)$:

$$\rho_{MM'} = \sum_{k,q} (-1)^{k-N-M} A_q^{(k)}(N) \times \langle kq | N-M, NM' \rangle . \qquad (5)$$

To provide an idea how the population of the individual M levels for our measured results appears, we have evaluated the above equation for $N=10$ assuming $A_{0+}^{\{1\}}=0.1$ and $A_{0+}^{\{2\}}=0.15$. Fig. 8 shows a graph of

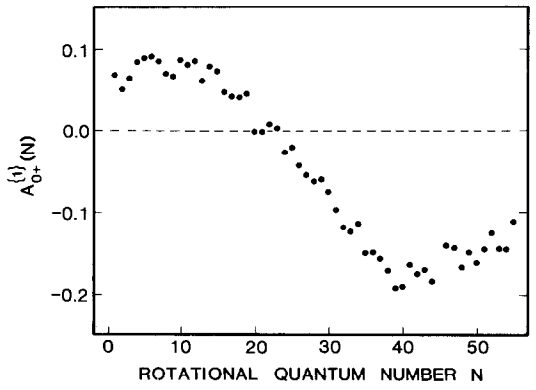

Fig. 7. Dipole orientation moment $A_{0+}^{\{1\}}(N)$ versus rotational quantum number N for the CN ($v=0$) photofragment in the photolysis of ICN by a beam of circularly polarized 248 nm light.

the population distribution obtained in this way. It exhibits a variation of population of the individual M states by a factor of 2. The minimum at $M=-3$ is caused by the positive value of $A_{0+}^{\{2\}}$.

We might also ask what is the maximum value for the orientation moment $A_{0+}^{\{1\}}$ which is in accord with the symmetry restrictions on the system. This will give us an idea of the orientation strength. In fact, the maximum value of $A_{0+}^{\{1\}}=\pm 1$ is not achievable when all the higher orientation moments equal zero. For $N=10$ and a quadrupole alignment moment of 0.15 (measured value), the maximum value for $A_{0+}^{\{1\}}$ is 0.47 before population distributions from eq. (5) become unphysical. This value should be compared to those given in fig. 7.

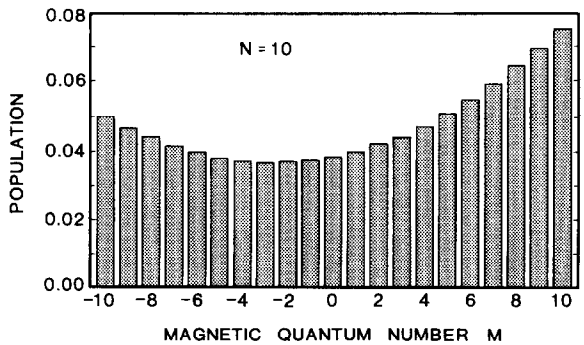

Fig. 8. Relative population of M states for $N=10$ when the dipole orientation moment has the value $A_{0+}^{\{1\}}=0.1$ and the quadrupole alignment moment the value $A_{0+}^{\{2\}}=0.15$.

5. Discussion

The photodissociation dynamics of ICN via its $\tilde{A}$ state continuum is known to be involved owing in part to two open channels:

$$\mathrm{ICN}+h\nu\rightarrow\mathrm{CN}(X\,^2\Sigma^+)+\mathrm{I}(^2P_{3/2})\,,$$
$$\rightarrow\mathrm{CN}(X\,^2\Sigma^+)+\mathrm{I}(^2P_{1/2})\,. \qquad (6)$$

The ground state of ICN may be described by the molecular orbital configuration

$$(1\sigma)^2(2\sigma)^2(3\sigma)^2(1\pi)^4(4\sigma)^2(2\pi)^4 \quad \tilde{X}\,^1\Sigma^+\,, \qquad (7)$$

where ICN is regarded as a 16-valence-electron system (7 from I, 4 from C, and 5 from N) [20,21]. The highest occupied molecular oribital (HOMO) is 2π; it is formed from atomic p orbitals on each atom which are in-phase between the carbon and nitrogen atoms but out-of-phase between the carbon and iodine atoms. The fact that the ionization potential of ICN (which involves removal of the 2π electron) is so close to that of I, suggests that the 2π molecular orbital is largely localized on the iodine atom. The lowest unoccupied molecular orbital (LUMO) is 5σ, which is strongly antibonding in the I–C region. Thus, the excited state is expected to have the configuration

$$(1\sigma)^2(2\sigma)^2(3\sigma)^2(1\pi)^4(4\sigma)^2(2\pi)^3(5\sigma)$$
$$\tilde{A}\,^{1,3}\Pi\,. \qquad (8)$$

The $\tilde{A}$–$\tilde{X}$ transition is thought to be of the type $2\pi\rightarrow5\sigma$ ($\pi\rightarrow\sigma^*$). The next highest configuration involves $\pi\rightarrow\pi^*$ type of promotion

$$(1\sigma)^2(2\sigma)^2(3\sigma)^2(1\pi)^4(4\sigma)^2(2\pi)^3(3\pi)$$
$$^{1,3}\Sigma^+,\,^{1,3}\Sigma^-,\,^{1,3}\Delta \qquad (9)$$

and it is expected that the energy of one or more of these states is lowered on bending of the ICN framework. Because of the large spin–orbit splitting of the iodine atom, the angular momentum coupling in ICN might be described best by Hund's case (c). However, the exact nature of the $\tilde{A}$ state continuum is presently unknown.

Several studies have examined the angular distribution and alignment of the CN fragment in the photodissociation of ICN by a beam of linearly polarized light [11,19,22,23]. In particular, Nadler et al. [11] measured the β parameter, which characterizes the anisotropy of the angular distribution. For photolysis at 266 nm, they found that β varies with N, the rotational quantum number of the CN($v=0$) fragment. Their angular distribution was determined from the shape of CN Doppler profile measurements. In addition to being able to extract the β parameters, they were also able to distinguish, from the differences in the width of the Doppler profiles, the CN fragments produced in correlation with $\mathrm{I}(^2P_{3/2})$ from those produced in correlation with $\mathrm{I}(^2P_{1/2})$. They found $\beta=1.6$ for low N (which correlated with $\mathrm{I}(^2P_{1/2})$) and $\beta=1.3$ for high N (which correlated with $\mathrm{I}(^2P_{3/2})$).

O'Halloran et al. [20] have determined the quadrupole alignment parameter $A_0^{\{2\}}(N)$ for the CN($v=0$) fragments and find a similar variation of $A_0^{\{2\}}(N)$ with N. They report that $A_0^{\{2\}}(N)$ changes gradually from about $A_0^{\{2\}}(N)=-0.28$ at low N to about $A_0^{\{2\}}=-0.12$ at high N.

O'Halloran et al. have put forward a model to account for the variation of both β and $A_0^{\{2\}}$ with N. It is proposed that at least two excited states are involved in the $\tilde{A}$ continuum dissociation of ICN: a linear state of ICN correlating with $\mathrm{I}(^2P_{1/2})$ and CN $X\,^2\Sigma^+$ with low values of N and a bent state of ICN correlating with $\mathrm{I}(^2P_{3/2})$ and CN $X\,^2\Sigma^+$ with high values of N. Arguments are presented that the curve crossing between the linear and bent surfaces takes place in the region of small I–CN separation, that is, in the Franck–Condon region directly above the well of the bound parent molecule. As a consequence, strong nonplanar interactions occur between the developing CN rotation $\boldsymbol{N}$ and the angular momentum $\boldsymbol{j}$ of the iodine atom. These nonplanar forces change the direction of both the velocity and angular momentum vector, causing a decrease in the magnitude of both the β parameter and the quadrupole alignment parameter $A_0^{\{2\}}$. Further evidence for this model is the observation of significant differences in the population of the F_1 and F_2 spin–rotation components of the CN $X\,^2\Sigma^+$ fragment, which changes with photolysis wavelength and with N [12].

In sharp contrast to the gradual variation of β and $A_0^{\{2\}}$ with N, the orientation of the CN($v=0$) fragment shows a marked dependence on N which even reverses sign. It would seem apparent that the $A_0^{\{1\}}$ orientation moment provides a more direct measure of the $\mathrm{I}(^2P_{1/2})/\mathrm{I}(^2P_{3/2})$ ratio. Indeed, in searching

for the origin of the orientation effect in CN we are led to the conclusion that the existence of spin–orbit (or spin–axis) interaction involving the I atom is necessary for the observation of photofragment orientation. Although we have no detailed theory for the observed photofragment orientation, this conclusion should not be so surprising if one examines the atomic physics counterpart of the present experiment, namely, the production of oriented (spin-polarized) electrons in the photoionization of an atom by a beam of circularly polarized light [5].

Consider photoionization of an alkali atom undergoing a one-photon transition from the ground state $^2S_{1/2}$ to the continuum channels $\epsilon\,^2P_{1/2,3/2}$ under the action of circularly polarized light. To be specific, let us choose the helicity of the light beam so that only $\Delta m_j = +1$ transitions occur – and denote the states by $|lm\rangle|sm_s\rangle$ (uncoupled representation). Then the ground state level $|00\rangle|\frac{1}{2}\ \frac{1}{2}\rangle$ is connected only to the $m_j = 3/2$ level of $\epsilon\,P_{3/2}$, namely, $|11\rangle|\frac{1}{2}\ \frac{1}{2}\rangle$. It should be recognized that this transition cannot change the orientation of the electron spin. However, the other $^2S_{1/2}$ ground state level $|00\rangle|\frac{1}{2}\ -\frac{1}{2}\rangle$ is connected to the $m_j = 1/2$ levels of $\epsilon\,^2P_{3/2}$ and $\epsilon\,^2P_{1/2}$, namely, to $[(2/3)^{1/2}|10\rangle|\frac{1}{2}\ \frac{1}{2}\rangle + (1/3)^{1/2}|11\rangle|\frac{1}{2}\ -\frac{1}{2}\rangle]$ and to $[(1/3)^{1/2}|10\rangle|\frac{1}{2}\ \frac{1}{2}\rangle - (2/3)^{1/2}|11\rangle|\frac{1}{2}\ -\frac{1}{2}\rangle]$, respectively. For this transition there is the opportunity for the electron spin to be "flipped" and the probability for this spin flip depends sensitively on the transition strengths (radial matrix elements) of these two different channels. Let us define the radial part of the electric dipole matrix element by

$$R_{1/2} = \langle \psi(^2P_{1/2}; r)\,|r|\,\psi(^2S_{1/2}; r)\rangle \tag{10}$$

and

$$R_{3/2} = \langle \psi(^2P_{3/2}; r)\,|r|\,\psi(^2S_{1/2}; r)\rangle \tag{11}$$

and let $N(\uparrow)$ and $N(\downarrow)$ denote the population of photoelectrons with spin up $|\frac{1}{2}\ \frac{1}{2}\rangle$ and spin down $|\frac{1}{2}\ -\frac{1}{2}\rangle$ integrated over all angles. Then it may be shown that [5]

$$\frac{N(\uparrow)-N(\downarrow)}{N(\uparrow)+N(\downarrow)} = \frac{9R_{3/2}^2+2(R_{3/2}-R_{1/2})^2-(2R_{1/2}+R_{3/2})^2}{9R_{3/2}^2+2(R_{3/2}-R_{1/2})^2+(2R_{1/2}+R_{3/2})^2}. \tag{12}$$

This expression demonstrates that spin polarization of the photoelectron vanishes when $R_{1/2} = R_{3/2}$, i.e. the presence of spin–orbit interaction is required for the production of spin-polarized photoelectrons.

An analogous argument must apply to the photolysis of ICN by a beam of circularly polarized light. The large spin–orbit splitting of the iodine atom fragment causes differential contributions to the possible continuum channels in the $2\pi \rightarrow 5\sigma$ excitation process. Polarization of the electron on the iodine atom also causes polarization of the electron on the CN fragment because the electron motions are correlated. Hence, the coupling of the electron spin on the iodine atom to be parallel $I(^2P_{3/2})$ or antiparallel $I(^2P_{1/2})$ with the electronic orbital angular momentum on the iodine atom also influences the sense of rotation that the CN fragment develops as the ICN system dissociates. It would be expected then that both the I and the CN fragments would be oriented in the photodissociaton of ICN by circularly polarized light [#2]. Theories for the degree of orientation for atomic fragments produced by the photodissociation of a diatomic molecule with a beam of circularly polarized light have been developed by several authors [24–27] and seem to support the above simple considerations. However, because the photodissociation dynamics of ICN via its $\tilde{A}$ state continuum is so complex, a deeper analysis has not been attempted here.

In conclusion, the production of oriented photofragments is the expected outcome when a sample of unpolarized molecules is photolyzed with a beam of circularly polarized light, provided that the fragments are open shell species having strong spin-dependent forces between them. Moreover, measurement of the degree of orientation provides a sensitive indicator of how these forces influence the dynamics of the recoil process as the photofragments separate.

Acknowledgement

We wish to thank Andrew C. Kummel for many helpful discussions and for providing us with the line

[#2] Unfortunately, the large nuclear spin of the iodine atom ($I = 5/2$) causes the expected degree of orientation to be greatly diminished (see ref. [3]). An attempt was made to measure the degree of orientation of the I atom using two-photon LIF at 304 nm. However, the results were inconclusive.

strength factors. This work was supported by the US National Science Foundation under NSF PHY 85-06668. EH thanks the Deutsche Forschungsgemeinschaft for a postdoctoral fellowship.

References

[1] M.N.R. Ashfold and J.E. Baggott, eds., Advances in gas-phase photochemistry and kinetics. Molecular photodissociation dynamics (Royal Society of Chemistry, London, 1987).
[2] Dynamics of Molecular Photofragmentation, Faraday Discussions Chem. Soc. 82 (1986) pp. 1–410.
[3] C.H. Greene and R.N. Zare, Ann. Rev. Phys. Chem. 33 (1982) 119.
[4] U. Heinzmann, in: Applications of circularly polarized radiation using synchrotron and ordinary sources, eds. F. Allen and C. Bustamante (Plenum Press, New York, 1985).
[5] J. Kessler, Polarized electrons (Springer, Berlin, 1976) ch. 5.
[6] N.A. Cherepkov, Advan. At. Mol. Phys. 19 (1983) 395.
[7] O.S. Vasyutinkskii, JETP Letters 31 (1980) 429; Opt. Spectry. (USSR) 51 (1981) 124; Soviet Tech. Phys. Letters 9 (1983) 404.
[8] R. Altkorn and R.N. Zare, Ann. Rev. Phys. Chem. 35 (1984) 265.
[9] R.N. Dixon, J. Chem. Phys. 85 (1986) 1866.
[10] G.E. Hall, N. Sivakumar, P.L. Houston and I. Burak, Phys. Rev. Letters 56 (1986) 1671.
[11] I. Nadler, D. Mahgerefteh, H. Reisler and C. Wittig, J. Chem. Phys. 82 (1985) 3885.
[12] H. Joswig, M. O'Halloran, R.N. Zare and M.S. Child, Faraday Discussions Chem. Soc. 82 (1986) 79.
[13] P.P. Feofilov, The physical basis of polarized emission (Consultants Bureau, New York, 1961).
[14] W. Demtröder, Laser spectroscopy (Springer, Berlin, 1981).
[15] A.C. Kummel, G.O. Sitz and R.N. Zare, J. Chem. Phys. 88 (1988) 7357.
[16] D.A. Case, G.M. McClelland and D.R. Herschbach, Mol. Phys. 35 (1978) 541.
[17] A.J. Bain and A.J. McCaffery, J. Chem. Phys. 80 (1984) 5883.
[18] I.V. Hertel and W. Stoll, Advan. At. Mol. Phys. 13 (1978) 113.
[19] M.A. O'Halloran, H. Joswig and R.N. Zare, J. Chem. Phys. 87 (1987) 303.
[20] J.M. Hollas and T.A. Sutherley, Mol. Phys. 22 (1971) 213.
[21] G.W. King and A.W. Richardson, J. Mol. Spectry. 21 (1966) 339.
[22] J.H. Ling and K.R. Wilson, J. Chem. Phys. 63 (1975) 101.
[23] G.E. Hall, N. Sivakumar and P.L. Houston, J. Chem. Phys. 84 (1986) 2120.
[24] Y.B. Band, K.F. Freed and S.J. Singer, J. Chem. Phys. 84 (1986) 3762.
[25] O.S. Vasyutinskii, Sov. Phys. JETP 54 (1981) 855; Opt. Spectry. (USSR) 51 (1981) 124; 54 (1983) 524.
[26] J. Vigué, J.A. Beswick and M. Broyer, J. Phys. (Paris) 44 (1983) 1225.
[27] M. Glass-Maujean and J.A. Beswick, Phys. Rev. A 36 (1987) 1170.